







# Modulated Model Predictive Speed Controller for PMSM Drives Employing Voltage-Based Cost Function

AHMED ABOELHASSAN <sup>1,2</sup> (Member, IEEE), SHUO WANG <sup>1</sup> (Member, IEEE),  
GIAMPAOLO BUTICCHI <sup>1</sup> (Senior Member, IEEE), VASYL VARVOLIK <sup>1</sup> (Member, IEEE),  
MICHAEL GALEA <sup>3</sup> (Senior Member, IEEE), AND SERHIY BOZHKO <sup>4</sup> (Senior Member, IEEE)

<sup>1</sup>Key Laboratory of More Electric Aircraft Technology of Zhejiang Province, University of Nottingham Ningbo China, Ningbo 315100, China

<sup>2</sup>Electrical and Control Engineering Department, College of Engineering and Technology, Arab Academy for Science, Technology, and Maritime Transport, Alexandria 1029, Egypt

<sup>3</sup>Department of Electrical Engineering, University of Malta, 2080 Msida, Malta

<sup>4</sup>University of Nottingham, NG7 2RD Nottingham, U.K.

CORRESPONDING AUTHOR: SHUO WANG (e-mail: shuo.wang@nottingham.edu.cn)

This work was supported by Zhejiang Basic and Commonweal Program under Project LQ23E070002.

**ABSTRACT** Various electrical drive systems have widely implemented the classical cascaded field-oriented control (FOC) topology, including speed loop, current loop, and modulation. On the other hand, modulated model predictive control (M<sup>2</sup>PC) has been employed recently for different applications for faster dynamic response and better power quality. The FOC topology's speed and current control loops can be merged to simplify the control system structure and improve the system dynamics. Therefore, a noncascaded speed loop controller employing M<sup>2</sup>PC for permanent magnet synchronous motors is introduced. The required simulation work has been developed to analyze the algorithm performance compared to proportional integral (PI), noncascaded model predictive control, and M<sup>2</sup>PC controllers. In addition, it has been applied practically through a dedicated testing rig, and results are investigated showing its merits including harmonic content, dynamic behavior, and robustness against parameter mismatch.

**INDEX TERMS** Modulated model predictive speed control (M<sup>2</sup>PSC), electrical drive applications, permanent magnet synchronous motor (PMSM) machine, voltage-based cost function.

## I. INTRODUCTION

Electrification of future transport systems has received growing interest over the last few decades to achieve higher system efficiency and reduce emissions. This trend results in an increased number of electrical drive systems that have been adopted in different transportation applications [1]. Consequently, the demand for improved electrical drive systems has increased as industry, energy, and transportation systems have evolved [2]. Permanent magnet synchronous motors (PMSMs) are employed in several applications because of their high power density, low maintenance cost, and high efficiency [3], [4].

PMSM drive system is considered a multi-input multi-output nonlinear system, and its control behavior can be influenced by several uncertain factors during operation, such

as parameters' variation, external load disturbance, cross coupling among  $dq$  current components, nonlinear dynamics, and unmodeled parameters of the system [5]. Additionally, the optimal performance of the PMSM electrical drive can be diminished if the time delay between feedback measurements and actuation is not considered. It would impact the control system's stability and restrict its bandwidth and dynamic performance [6]. The time delay is caused by the controller's digital computational period and the power electronics converter as modulation signals are generated at the initial stage of each sampling period and require one cycle to be fully applied [7].

On the other hand, speed control is essential for the electric drive system to enhance its performance and efficiency throughout different operating conditions and load variations

[8]. Deferent techniques have been proposed in the literature to perform the PMSM speed loop control better. An adaptive PID controller based on the gradient descent method has been proposed in [8]. Moreover, a robust speed controller is presented in [9] employing the disturbance observer approach. A sliding mode control is given in [10] for dual PMSM parallel operation. Besides, an active disturbance rejection control for current and speed loops is developed in [11] for PMSM, while virtual cogging torque control is used to reduce the speed ripples in [12].

Model predictive control (MPC) has been acknowledged as one of the most effective techniques to emerge from modern control theory into industrial applications [13]. It has been successfully applied for speed control of PMSM [14], [15], [16], and induction motor drives [17]. MPC can be developed based on a short prediction horizon of  $n_y$  equal to 1 or a long prediction horizon of  $n_y \geq 2$  [18]. The proper selection of the  $n_y$  value is important and considered as a direct approach to overcome the mentioned time delay issues. However, the model computational burden should be considered as it would be challenging for practical implementation in case of long prediction horizons [19].

The performance of the MPC controller can be enhanced by adapting the cost function weighting factors online or eliminating the steady-state error (SSE) from the system variables. In [20], the given preexisting error of the system variable is considered to adapt the cost function weighting factors dynamically. Furthermore, an artificial neural network algorithm is implemented in [21] to adapt the weighting factors for the control of a power converter online. To mitigate the estimated SSE of grid-connected multilevel converter controlled variables, the MPC control scheme has been modified in [22] to eliminate the system model uncertainties. The system transfer function has been reformed in [23] to the resonant form to improve the steady state operation for the fault-tolerant control of multiphase PMSM machine.

One of the recently introduced MPC topologies is the modulated model predictive control (M<sup>2</sup>PC) [24], [25]. It employs the finite set MPC with the space vector pulsewidth modulation (SVPWM). The optimal voltage vector will be investigated by calculating all given voltage vectors of the power converter for improved operation and higher power quality [26]. It has been implemented successfully in several applications and systems including a three-phase rectifier [27], direct matrix converter [28], multilevel converter for PMSM [25], and multiphase induction motor drive [29].

Considering the merits of the M<sup>2</sup>PC controller, a modulated model predictive speed control (M<sup>2</sup>PSC) approach is proposed for an enhanced PMSM speed control behavior and overall electrical drive operation. The speed and current control loops will be combined to execute the whole control system at the same sampling time, resulting in faster dynamic response and improved operation compared to the conventional field-oriented control (FOC) structure. The reference  $dq$  voltages will be calculated including the system constraints with an adequate prediction window considering the system

time delay. The applied switching patterns will be decided according to the proposed voltage-based cost function, which is the article's main contribution. Besides, an integrator has been implemented to adapt the speed weighting factor to eliminate the SSE throughout different operating conditions for a more robust speed response performance. In addition, an extended state observer (ESO) is introduced for load torque estimation.

The rest of the article is organized as follows. The PMSM mathematical model and its linearization are addressed in Section II followed by the equations of the proposed strategy. Section III is devoted to the simulation results and analysis of the given strategy compared to the common MPC, M<sup>2</sup>PC, and proportional integral (PI) controllers. The description of the testing bench and the maintained practical results are illustrated in Section IV, while Section V concludes this article.

## II. M<sup>2</sup>PSC STRATEGY

### A. PMSM MATHEMATICAL MODEL

It is necessary to present the PMSM model first as MPC is a model-based control strategy. The differential equations of PMSM are given by the following [30]:

$$\frac{d}{dt}i_d = \frac{1}{L_d}(v_d - R_s i_d + L_q i_q \omega_e) \quad (1)$$

$$\frac{d}{dt}i_q = \frac{1}{L_q}(v_q - R_s i_q - L_d i_d \omega_e - \varphi_f \omega_e) \quad (2)$$

$$\frac{d}{dt}\omega_e = \frac{p}{J}\left(T_e - \frac{B_y}{p}\omega_e - T_L\right) \quad (3)$$

$$T_e = \frac{3p}{2}(\varphi_f i_q + (L_d - L_q)i_d i_q) \quad (4)$$

where  $v_d$ ,  $v_q$  are  $dq$  stator voltage components,  $i_d$ ,  $i_q$  are  $dq$  stator current components,  $L_d$ ,  $L_q$  are  $dq$  synchronous inductances,  $\varphi_f$  is the stator-rotor flux,  $\omega_e$  is the electrical angular velocity,  $R_s$  is the stator resistance,  $p$  is pole pairs,  $T_e$  is the electromagnetic torque,  $T_L$  is the load torque,  $J$  is the moment of inertia, and  $B_y$  is the friction coefficient.

Since the model is nonlinear, it is required to be linearized around a definite operating point using Taylor expansion. The linearized equations can be illustrated as follows:

$$i_q \omega_e = \omega_{e0} i_{q0} + i_{q0}(\omega_e - \omega_{e0}) + \omega_{e0}(i_q - i_{q0}) \quad (5)$$

$$i_d \omega_e = \omega_{e0} i_{d0} + i_{d0}(\omega_e - \omega_{e0}) + \omega_{e0}(i_d - i_{d0}) \quad (6)$$

where  $\omega_{e0}$ ,  $i_{d0}$ , and  $i_{q0}$  are the operating point values of the linearized model. By substituting (1) and (2) with (5) and (6), the linearized PMSM state-space model is given by the following:

$$\dot{\mathbf{x}}(t) = \mathbf{A}_m \mathbf{x}(t) + \mathbf{B}_m \mathbf{u}(t) + \boldsymbol{\delta}_m \quad (7)$$

$$\mathbf{y}(t) = \mathbf{C}_m \mathbf{x}(t) + \mathbf{D}_m \mathbf{u}(t) \quad (8)$$

where

$$\mathbf{x}(t)^T = [i_d \quad i_q \quad \omega_e]$$

$$\mathbf{u}(t)^T = [v_d \quad v_q]$$

$$\mathbf{y}(t)^T = [i_d \quad i_q \quad \omega_e]$$

$$\mathbf{A}_m = \begin{bmatrix} -\frac{R_s}{L_d} & \frac{L_q}{L_d}\omega_e0 & \frac{L_q}{L_d}i_{q0} \\ -\frac{L_d}{L_q}\omega_e0 & -\frac{R_s}{L_q} & -\left(\frac{L_d}{L_q}i_{d0} + \frac{\varphi_f}{L_q}\right) \\ 0 & \frac{3p^2\varphi_f}{2J} & -\frac{B_y}{J} \end{bmatrix}$$

$$\mathbf{B}_m = \begin{bmatrix} 1/L_d & 0 \\ 0 & 1/L_q \\ 0 & 0 \end{bmatrix}$$

$$\boldsymbol{\delta}_m = \begin{bmatrix} -\frac{L_q}{L_d}\omega_e0i_{q0} \\ \frac{L_d}{L_q}\omega_e0i_{d0} \\ -\frac{pT_L}{J} \end{bmatrix}$$

$$\mathbf{C}_m = \begin{bmatrix} 1 & 0 & 0 \\ 0 & 1 & 0 \\ 0 & 0 & 1 \end{bmatrix}$$

$$\mathbf{D}_m = 0.$$

This model is discretized with a definite sampling time  $T_s$  using the forward Euler approximation method. The discretized state-space model of the system is as follows:

$$\mathbf{x}(k+1) = \mathbf{A}\mathbf{x}(k) + \mathbf{B}\mathbf{u}(k) + \boldsymbol{\delta} \quad (9)$$

$$\mathbf{y}(k) = \mathbf{C}\mathbf{x}(k) + \mathbf{D}\mathbf{u}(k) \quad (10)$$

where

$$\mathbf{A} = \mathbf{I} + \mathbf{A}_m T_s = \begin{bmatrix} \left(1 - \frac{R_s T_s}{L_d}\right) & \frac{L_q T_s \omega_e0}{L_d} & \frac{L_q T_s i_{q0}}{L_d} \\ -\frac{L_d T_s \omega_e0}{L_q} & \left(1 - \frac{R_s T_s}{L_q}\right) & -T_s \left(\frac{L_d}{L_q} i_{d0} + \frac{\varphi_f}{L_q}\right) \\ 0 & T_s \left(\frac{3p^2 \varphi_f}{2J}\right) & \left(1 - \frac{B_y T_s}{J}\right) \end{bmatrix}$$

$$\mathbf{B} = \mathbf{B}_m T_s = \begin{bmatrix} T_s/L_d & 0 \\ 0 & T_s/L_q \\ 0 & 0 \end{bmatrix}$$

$$\boldsymbol{\delta} = \boldsymbol{\delta}_m T_s = \begin{bmatrix} -T_s \omega_e0 i_{q0} \\ T_s \omega_e0 i_{d0} \\ -T_s \left(\frac{pT_L}{J}\right) \end{bmatrix}$$

$$\mathbf{C} = \mathbf{C}_m$$

$$\mathbf{D} = \mathbf{D}_m.$$

## B. COST FUNCTION

The M<sup>2</sup>PSC controller will replace the PI controllers of the FOC topology to achieve the proposed method. The following cost function will be calculated for each voltage vector:

$$g = (u_d(k) - v_d(k))^2 + (u_q(k) - v_q(k))^2 \quad (11)$$

where  $\mathbf{u}_{dq}(k)$  will be calculated by solving the following equation [31]:

$$\mathbf{j} = \sum_{k=1}^{n_y} \mathbf{e}^T(k) \mathbf{Q}(k) \mathbf{e}(k) + \sum_{k=0}^{n_u-1} \mathbf{u}_{dq}^T(k) \mathbf{R}(k) \mathbf{u}_{dq}(k). \quad (12)$$

$\mathbf{j}$  is subjected to a discretized and linearized PMSM state-space model in (9) and (10), where  $\mathbf{e}(k) = \mathbf{y}(k) - \mathbf{r}(k)$  is the  $(l * 1)$  error,  $\mathbf{y}(k)$  is the  $(l * 1)$  system output,  $\mathbf{r}(k)$  is the  $(l * 1)$  reference input,  $\mathbf{u}_{dq}(k)$  is the  $(m * 1)$  optimal voltage vector,  $\mathbf{Q}(k)$  and  $\mathbf{R}(k)$  are  $(l * l)$ ,  $(m * m)$  weighting matrices,  $m$  is the number of inputs,  $l$  is the number of outputs,  $n$  is the number of states, and  $n_u$  is the control horizon. The model can be employed recursively to find the predictions over the prediction horizon  $n_y$  to overcome the delay effects, for instance

$$\hat{\mathbf{x}}(k+1) = \mathbf{P}_x \mathbf{x}(k) + \mathbf{H}_x \hat{\mathbf{u}}_{dq}(k) \quad (13)$$

$$\hat{\mathbf{y}}(k+1) = \mathbf{P} \mathbf{x}(k) + \mathbf{H} \hat{\mathbf{u}}_{dq}(k) \quad (14)$$

where

$$\hat{\mathbf{x}}(k+1) = \begin{bmatrix} \mathbf{x}(k+1) \\ \mathbf{x}(k+2) \\ \mathbf{x}(k+3) \\ \vdots \\ \mathbf{x}(k+n_y) \end{bmatrix}, \quad \mathbf{P}_x = \begin{bmatrix} \mathbf{A} \\ \mathbf{A}^2 \\ \mathbf{A}^3 \\ \vdots \\ \mathbf{A}^{n_y} \end{bmatrix}$$

$$\mathbf{H}_x = \begin{bmatrix} \mathbf{B} & 0 & 0 & \dots \\ \mathbf{AB} & \mathbf{B} & 0 & \dots \\ \mathbf{A}^2\mathbf{B} & \mathbf{AB} & \mathbf{B} & \dots \\ \vdots & \vdots & \vdots & \vdots \\ \mathbf{A}^{n_y-1}\mathbf{B} & \mathbf{A}^{n_y-2}\mathbf{B} & \mathbf{A}^{n_y-3}\mathbf{B} & \dots \end{bmatrix}$$

$$\hat{\mathbf{u}}_{dq}(k) = \begin{bmatrix} \mathbf{u}_{dq}(k) \\ \mathbf{u}_{dq}(k+1) \\ \mathbf{u}_{dq}(k+2) \\ \vdots \\ \mathbf{u}_{dq}(k+n_y-1) \end{bmatrix}$$

$$\hat{\mathbf{y}}(k+1) = \begin{bmatrix} \mathbf{y}(k+1) \\ \mathbf{y}(k+2) \\ \mathbf{y}(k+3) \\ \vdots \\ \mathbf{y}(k+n_y) \end{bmatrix}; \quad \mathbf{P} = \begin{bmatrix} \mathbf{CA} \\ \mathbf{CA}^2 \\ \mathbf{CA}^3 \\ \vdots \\ \mathbf{CA}^{n_y} \end{bmatrix}$$

$$\mathbf{H} = \begin{bmatrix} \mathbf{CB} & 0 & 0 & \dots \\ \mathbf{CAB} & \mathbf{CB} & 0 & \dots \\ \mathbf{CA}^2\mathbf{B} & \mathbf{CAB} & \mathbf{CB} & \dots \\ \vdots & \vdots & \vdots & \vdots \\ \mathbf{CA}^{n_y-1}\mathbf{B} & \mathbf{CA}^{n_y-2}\mathbf{B} & \mathbf{CA}^{n_y-3}\mathbf{B} & \dots \end{bmatrix}.$$

$\hat{\mathbf{x}}(k+1)$  is the  $(n * n_y) * 1$  predicted system states, while  $\hat{\mathbf{y}}(k+1)$  is the  $(l * n_y) * 1$  system output,  $\hat{\mathbf{u}}_{dq}(k)$  is the  $(m * n_y) * 1$  optimal voltage vector, and  $\mathbf{P}_x$ ,  $\mathbf{H}_x$ ,  $\mathbf{P}$ ,  $\mathbf{H}$  are the  $(n * n_y) * n$ ,  $(n * n_y) * (m * n_y)$ ,  $(l * n_y) * n$ ,  $(l * n_y) * (m * n_y)$ .

$(m * n_y)$  system parameters all over  $n_y$ . The result of minimizing (11) for  $\mathbf{u}_{dq}(k)$  is given by the following:

$$\mathbf{u}_{dq}(k) = \mathbf{L}[(\mathbf{H}^T \hat{\mathbf{Q}}(k)\mathbf{H} + \mathbf{H}^T \hat{\mathbf{Q}}^T(k)\mathbf{H} + 2\hat{\mathbf{R}}^T(k))^{-1} 2\mathbf{H}^T \hat{\mathbf{Q}}^T(k)(\hat{\mathbf{r}}(k) - \mathbf{P}\mathbf{x}(k))] \quad (15)$$

where  $\mathbf{L} (m * (m * n_y)) = [\mathbf{I} : \mathbf{O}]$ ,  $\mathbf{I}$  is an  $(m * m)$  identity matrix, and  $\mathbf{O}$  is a  $m * (m * n_y - m)$  zero matrix,  $\hat{\mathbf{r}}(k)$  is the  $(l * n_y) * 1$  system reference,  $\hat{\mathbf{Q}}(k)$  and  $\hat{\mathbf{R}}(k)$  are  $(l * n_y) * (l * n_y)$ ,  $(m * n_u - 1) * (m * n_u - 1)$  weighting matrices. System input constraints have been considered for the given calculations such as

$$u_{\min} \leq \mathbf{u}_{dq}(k) \leq u_{\max} \quad (16)$$

where  $u_{\max}$  is  $v_{dc}/2$  and  $u_{\min}$  is  $-v_{dc}/2$ .

The duty cycles for the active vectors,  $d_i$  and  $d_j$ , and the zero vector,  $d_0$ , will be calculated such as follows [24]:

$$d_i = \left| \frac{u_q(k) s_d^j(k) - u_d(k) s_q^j(k)}{v_{dc} (s_d^j(k) s_q^i(k) - (s_d^i(k) s_q^j(k)))} \right| \quad (17)$$

$$d_j = \left| \frac{u_q(k) s_d^i(k) - u_d(k) s_q^i(k)}{v_{dc} (s_d^i(k) s_q^j(k) - (s_d^j(k) s_q^i(k)))} \right| \quad (18)$$

$$d_0 = 1 - d_i - d_j. \quad (19)$$

$v_{dc}$  is the applied dc voltage,  $i = 1, 2, \dots, 5, 6$ , and  $j = 2, 3, \dots, 6, 1$ . The  $s_{sq}(k)$  matrix can be defined as follows:

$$s_{sq}(k) = \begin{bmatrix} s_1 & s_1 + s_2 & s_2 & s_2 + s_3 & s_3 & s_1 + s_3 \\ s_4 & s_4 + s_5 & s_5 & s_5 + s_6 & s_6 & s_4 + s_6 \end{bmatrix} \quad (20)$$

where  $s_1, s_2, s_3, s_4, s_5$ , and  $s_6$  equal  $(\frac{2}{3} \cos \theta)$ ,  $(-\frac{1}{3} \cos \theta + \frac{\sqrt{3}}{3} \sin \theta)$ ,  $(-\frac{1}{3} \cos \theta - \frac{\sqrt{3}}{3} \sin \theta)$ ,  $(-\frac{2}{3} \sin \theta)$ ,  $(\frac{1}{3} \sin \theta + \frac{\sqrt{3}}{3} \cos \theta)$ , and  $(\frac{1}{3} \sin \theta - \frac{\sqrt{3}}{3} \cos \theta)$ . The timing for the applied voltage vector can be calculated as follows [28]:

$$t_x = d_x T_s \quad (21)$$

where  $x = i, j$ , or 0, then

$$t_i + t_j + t_0 = T_s. \quad (22)$$

The final cost function will be

$$g_{M^2PSC} = d_i g_i + d_j g_j. \quad (23)$$

The cost function given in (23) will be considered to find the optimal switching patterns to achieve the given  $\mathbf{u}_{dq}(k)$  in (15) as presented in Fig. 1. The three-phase modulation signals will be calculated based on the timing calculations in (21) of the optimal sector as illustrated in Fig. 2.

### C. WEIGHTING FACTOR ADAPTATION

Another improvement has been included for a more robust operation of the proposed controller. An integrator loop is implemented to provide an online adaptation of the speed

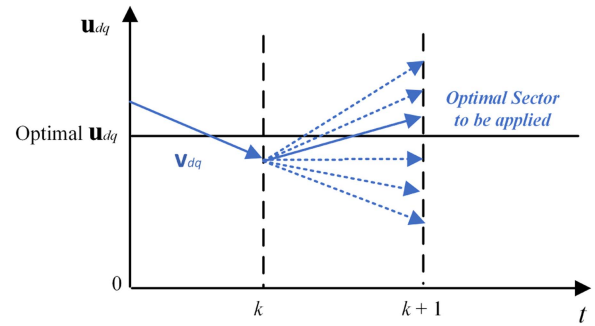


FIGURE 1. Proposed cost function concept.

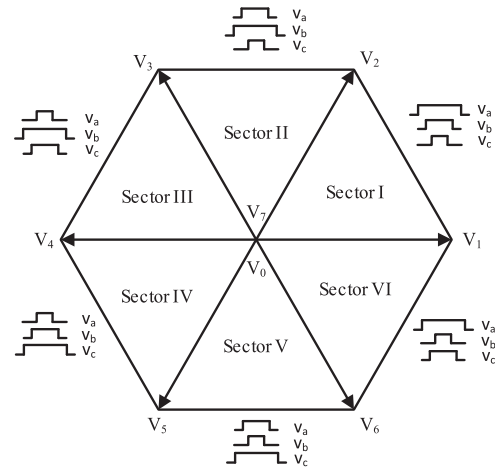


FIGURE 2. SVPWM voltage vectors.

weighting factor given at (15). The expression for  $Q_3(k)$  based on the forward Euler method is given by the following:

$$Q_3(k) = Q_3(k-1) + k_i T_s (\omega_m^*(k-1) - \omega_m(k-1)) \quad (24)$$

where  $k_i$  is the integrator gain,  $\omega_m^*$  is the reference mechanical angular velocity, and  $\omega_m$  is the mechanical angular velocity. As a result, the weighting factor will be modified to eliminate the SSE from the speed response and to improve the speed response against load disturbances among different operating conditions. It provides a reasonable solution for the weighting factor adaptation and is easy to implement considering the overall strategy's calculation burden.

### D. EXTENDED STATE OBSERVER DESIGN

After eliminating the cascaded FOC loops, it is required to provide the reference value for the quadrature current component as the speed PI controller is not given. An ESO is implemented to estimate the load torque value based on the measured  $i_q$  and  $\omega_m$  [32]. The observer gains have been designed based on the standard characteristics equation of the second-order system. Considering friction coefficient  $B_y$  equals zero, then the reference value for the quadrature current

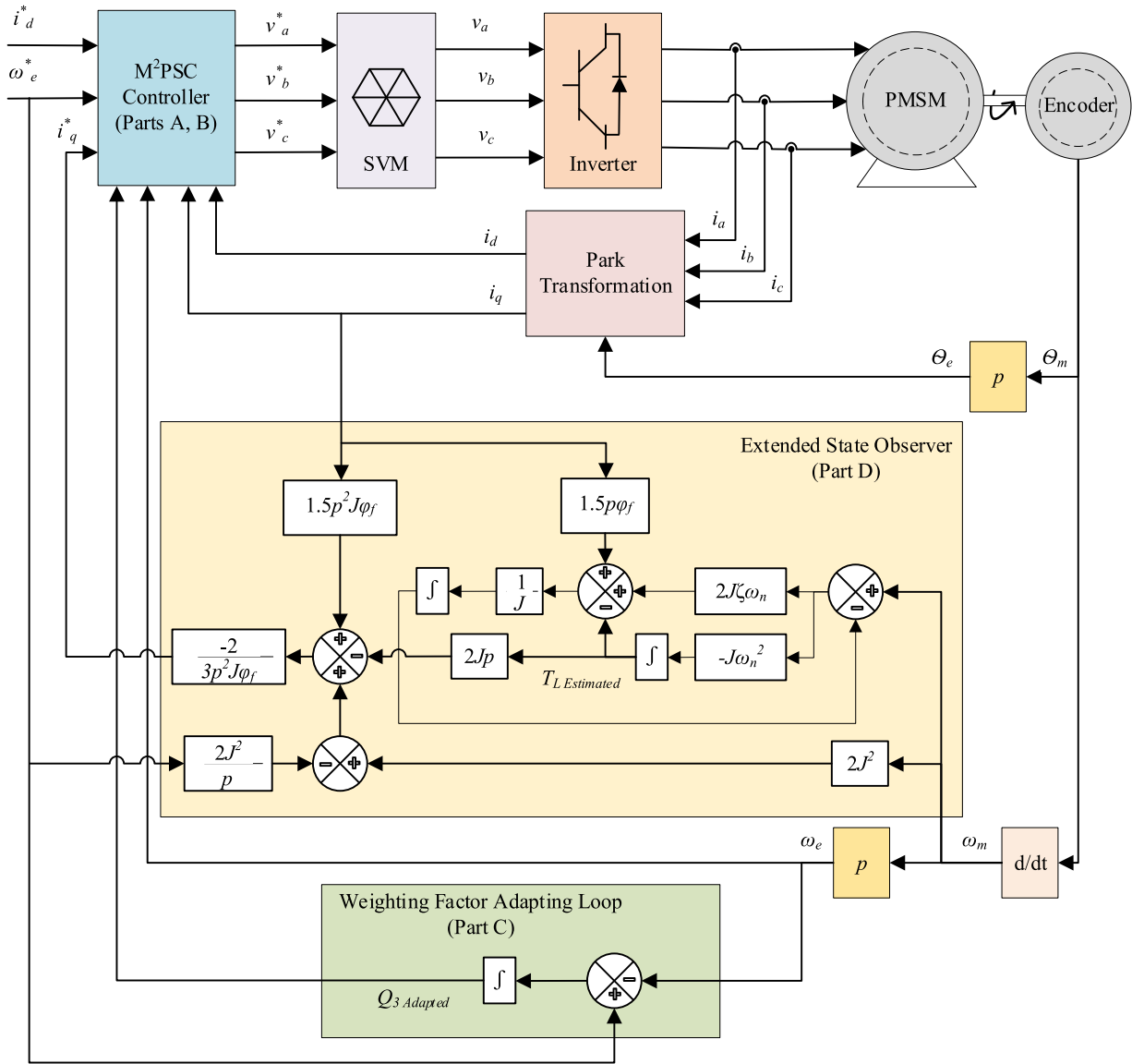


**FIGURE 3.** Proposed M<sup>2</sup>PSC strategy.

component  $i_q^*$  can be calculated such as [33]

$$i_q^* = \frac{-2}{3p^2 J \varphi_f} (2J^2 \omega_m - 2J^2 \omega_m^* - 2JpT_{L\text{Estimated}} + 1.5p^2 J \varphi_f i_q) \quad (25)$$

where  $T_{L\text{Estimated}}$  is the estimated load torque. The block diagram of the proposed strategy is illustrated in Fig. 3. The blue part combines the mathematical model and cost function operations, the weighting factor adapting loop is highlighted in green, while the yellow part includes the ESO and  $i_q^*$  calculations.

### III. SIMULATION RESULTS

To assess the addressed control method and loops, simulations were conducted using MATLAB/Simulink. Table 1 lists the parameters of the surface-mounted PMSM machine used in

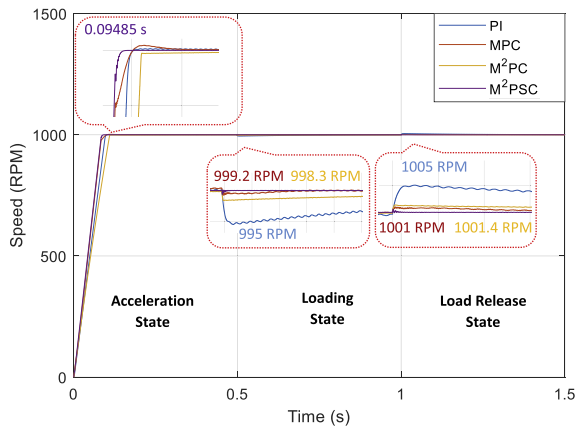
this analysis. Discrete-time blocks are used to illustrate control methods, and the inverter's switching model is employed to simulate the inverter at a dc bus voltage of 220 V. When the reference voltage is applied from the controller to the machine, a step time delay is considered. The resistive voltage drop across diodes, transistors, and the dead time have been overlooked. Besides, 10 kHz has been chosen for the switching frequency as an applicable value for most of the available inverters in the market. The control system dynamics were examined during a step change in the mechanical load to investigate the system performance. Both prediction and control horizons are settled for three samples to provide an acceptable prediction window and calculation burden.

Fig. 4 shows the speed behavior of the proposed strategy, PI, noncascaded MPC, and M<sup>2</sup>PC controllers against a load torque of 2 N·m at an operating speed of 1000 r/min. Based on the pole-zero cancellation technique, the PI current



**TABLE 1. PMSM Parameters**

Symbol	Parameter	Value
$P$	Rated Power	2.3 kW
$T_m$	Nominal Torque	15 Nm
$N_s$	Nominal Speed	1500 RPM
$I_{ph}$	Rated Phase Current	9.5 A
$v_{dc}$	DC Link Voltage	220 V
$R_s$	Phase Resistance	0.58625 $\Omega$
$L_d$	Direct Inductance	2.502067 mH
$L_q$	Quadrature Inductance	2.53605 mH
$p$	Pole Pairs	4
$\varphi_f$	PM Flux	0.395459 Wb
$J$	Total Inertia	0.00277 kgm <sup>2</sup>



**FIGURE 4. Speed response for the given strategies.**

controller has been finetuned. To get the highest dynamic performance for the PI controller and higher disturbance rejection with minimal overshoot, the bandwidth has been chosen to be 0.33 of the switching frequency, as shown by the equations  $k_p = \omega_o * l$  and  $k_i = \omega_o * r$ , given that  $\omega_o$  is the controller bandwidth [34]. For PI and M<sup>2</sup>PC controllers, the speed loop has been controlled using the same gains.

The system has achieved faster dynamic response by 0.09485 s without overshoot or SSE for the given strategy compared to 0.1021, 0.1387, and 0.1103 s for PI, MPC, and M<sup>2</sup>PC controllers, respectively. An overshoot of 0.065% is noticed for the PI controller and 0.2% for the MPC controller. Moreover, a step change to the load torque of 2 N·m has been applied at  $t = 0.5$  s. The proposed strategy provides an improved response against load disturbance compared to other methods. The PI controller gives under and overshoots of 0.5%, 0.08%, and 0.1% for MPC, while M<sup>2</sup>PC shows 0.17% and 0.14% against load variations.

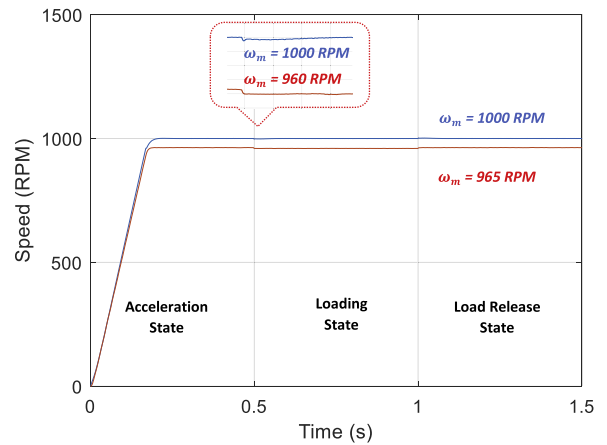


**FIGURE 5. M<sup>2</sup>PSC strategy with (blue) and without (red) the weighting factor adaptation.**

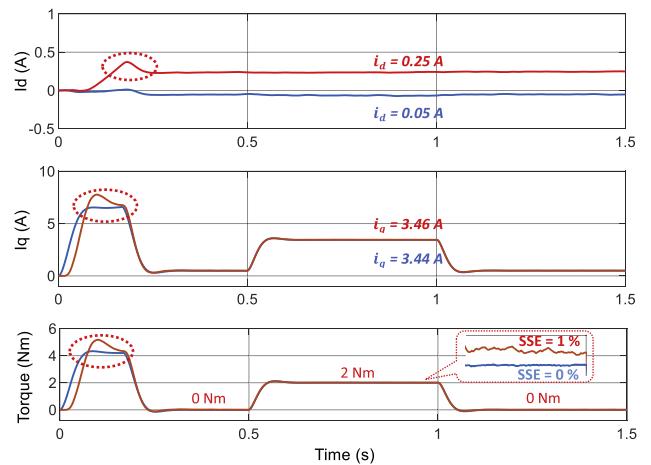


**FIGURE 6. M<sup>2</sup>PSC strategy with (blue) and without (red) the ESO loop.**

The effectiveness of the implemented ESO and integrator for speed weighting factor adaptation loops have been verified during the same loading and operating condition. In Fig. 5, the system has reached the speed operating point of 1000 r/min without SSE while achieving 960 r/min without the online adaptation. Additionally, the speed has dropped under loading condition leading to higher SSE in contrast to the robust behavior based on the implemented integrator loop. On the other hand, the torque and  $i_{dq}$  components show better behavior during the PMSM acceleration state employing the employed ESO as illustrated in Fig. 6. The torque has zero SSE throughout the loading condition, while it is 1% without the given ESO loop. Furthermore, the  $i_d$  component has an SSE of 0.25 A, while it is 0.05 A through the given ESO loop.

## IV. EXPERIMENTAL RESULTS

### A. PERFORMANCE ANALYSIS

The proposed strategy has been evaluated and compared with other controllers through the illustrated testing rig in Fig. 7 for the same surface-mounted PMSM machine model given in Table 1. The control system is developed based on the

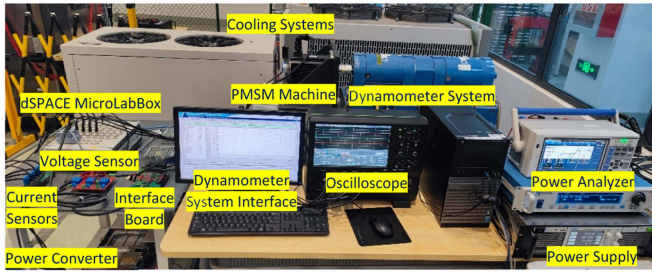


FIGURE 7. Experimental testing rig.

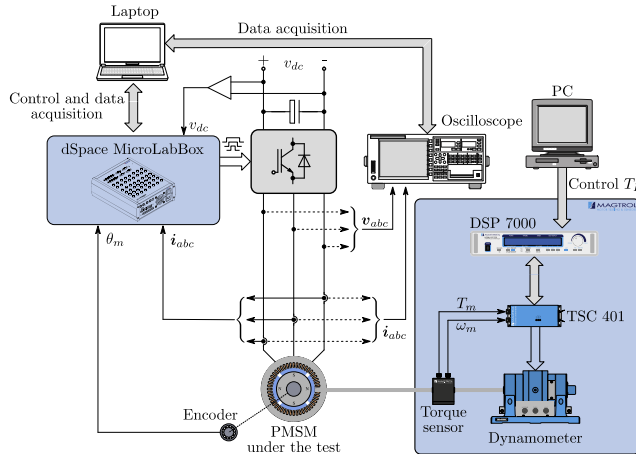


FIGURE 8. Block diagram of the experimental test rig.

dSPACE MicroLabBox controller. The given values for switching frequency, prediction, and control horizons in the simulation work are considered. An interface board is introduced to amplify the PWM signals from the dSPACE to the required level of the three-phase two-level IGBT SKAI inverter at a dc bus voltage of 220 V. In addition, it provides the necessary electric isolation between the power converter and the dSPACE controller. Three-phase current measurements are maintained throughout LEM current transducers. Moreover, an LEM voltage transducer is employed for the dc bus voltage measurement. A Magtrol dynamometer system is used to brake the PMSM motor. The proposed strategy computational time is  $22.36 \mu\text{s}$ . A block diagram for the experimental test rig is presented in Fig. 8.

Fig. 9 shows the speed response of the PI, noncascaded MPC,  $M^2PC$ , and  $M^2PSC$  controllers. The proposed strategy shows a faster dynamic response and reaches a speed of 1000 r/min without overshoot compared to 2% for MPC, 4.9% for  $M^2PC$ , and 5.7% for PI controllers. A load torque of 2 N·m is applied at  $t = 5$  s. The proposed strategy gives a robust speed response against load torque disturbance without under or overshoot. In contrast, under and overshoots of 3.1% and 4.6% are noticed for PI, and 3.4% and 5.2% for  $M^2PC$  methods under load variations. The adaptation of the speed weighting factor of the proposed strategy for the given speed behavior in Fig. 9 is presented in Fig. 10. The  $Q_3$  value is adapted according to the system behavior resulting in a robust

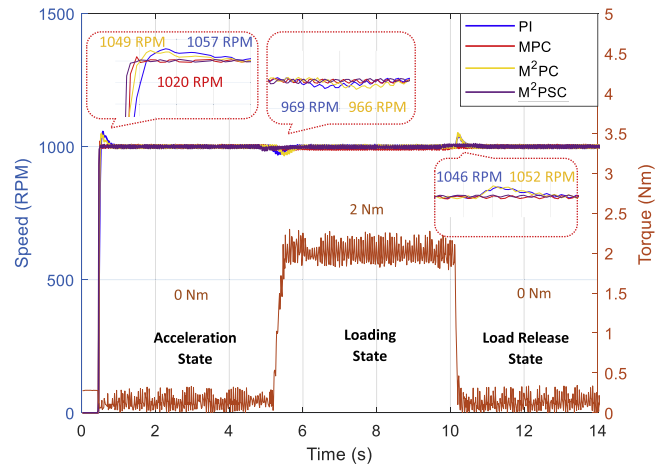


FIGURE 9. Speed response against the applied torque.

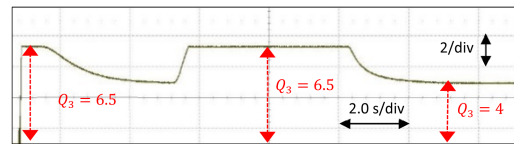


FIGURE 10. Adapted weighting factor behavior.

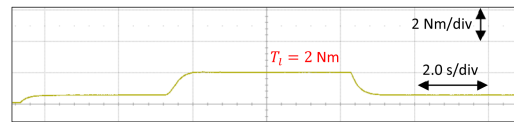


FIGURE 11. Estimated load torque.

response for the PMSM speed, while the estimated load torque is illustrated in Fig. 11.

Besides, Fig. 12 illustrates the current loop response of direct and quadrature components during the system loading for the given strategies. The proposed strategy shows a zero SSE for the  $I_d$  component compared to 1.5 A for the MPC controller throughout the loading condition. A speed step change is performed at  $t = 0.5$  s from 500 to 1000 r/min considering a 2 N·m load as given in Fig. 13. The proposed strategy shows a faster response than other methods. Overshoots of 3% and 3.3% are noticed for PI and  $M^2PC$  controllers, respectively, while the MPC controller achieved a slower response by 0.6230 s.

## B. THD ANALYSIS

A total harmonic distortion (THD) evaluation has been performed for phase “a” current considering the same operating condition of 1000 r/min and 2 N·m. The proposed methodology shows lower current distortion with a THD percentage of 5.65% in contrast to 9.48% and 7.82% for PI and MPC controllers, respectively. However,  $M^2PC$  gives a slightly lower THD by 0.1%. Fast Fourier transfer (FFT) analysis for the given strategies is illustrated in Fig. 14. The THD analysis outcomes are summarized in Table 2.





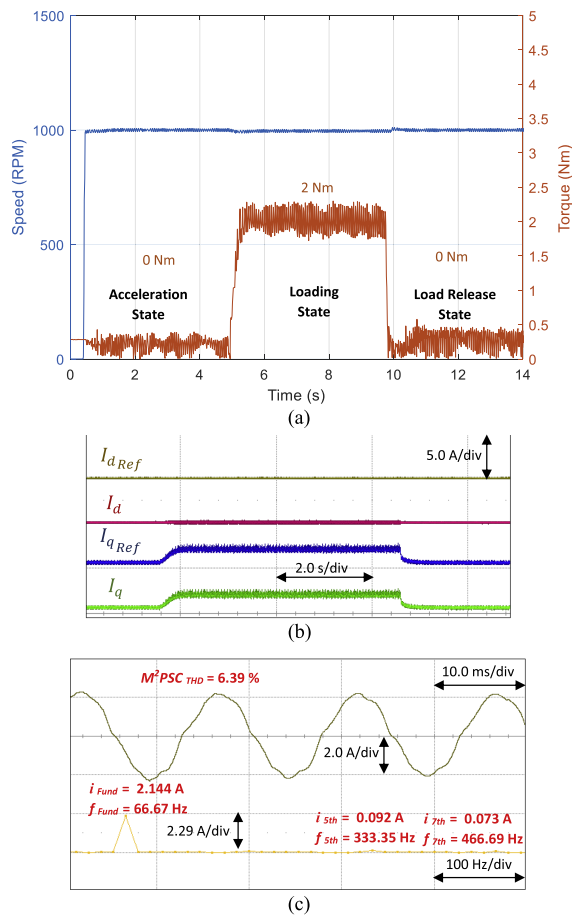


**FIGURE 15.** (a) Speed response, (b) current loops response, and (c) FFT analysis for phase “a” current under parameter mismatch of 50% for  $R_s$  and 5% for  $L_{dq}$  for the proposed strategy.

## V. CONCLUSION

A speed control method employing modulated model predictive control has been presented. The speed weighting factor of the cost function is online tuned to eliminate the SSE from the speed response. Additionally, an ESO is provided for the load torque estimation for a more robust operation. The simulation and practical results prove the proposed method’s ability to have an error-free speed performance and faster dynamic response under different operating conditions compared to predictive and PI strategies. The weighting factor and estimated torque curves proved the successful implementation of the controller loops and reflected in system performance. Besides, the proposed method offered a robust behavior in the presence of a parameter mismatch in the system model.

## REFERENCES

- [1] X. Lang, T. Yang, Z. Huang, Z. Wang, S. Bozhko, and P. Wheeler, “Instantaneous power control within an advanced power generation center for more-electric aircraft applications,” *IEEE Trans. Transp. Electric.*, vol. 8, no. 3, pp. 3261–3274, Sep. 2022.
- [2] A. M. Diab, S. Bozhko, M. Galea, and C. Gerada, “Stable and robust design of active disturbance-rejection current controller for permanent magnet machines in transportation systems,” *IEEE Trans. Transp. Electric.*, vol. 6, no. 4, pp. 1421–1433, Dec. 2020.

- [3] A. A. A. Abdelrauf, W. W. Saad, A. Hebala, and M. Galea, “Model predictive control based PID controller for PMSM for propulsion systems,” in *Proc. IEEE Int. Conf. Elect. Syst. Aircr., Railway, Ship Propulsion Road Veh. Int. Transp. Electric. Conf.*, 2018, pp. 1–7, doi: [10.1109/ESARS-ITEC.2018.8607585](https://doi.org/10.1109/ESARS-ITEC.2018.8607585).
- [4] A. M. Diab et al., “Performance analysis of complex vector discrete current controller for high-speed permanent magnet machines,” in *Proc. IEEE 17th Conf. Ind. Electron. Appl.*, 2022, pp. 590–595, doi: [10.1109/ICIEA54703.2022.10005975](https://doi.org/10.1109/ICIEA54703.2022.10005975).
- [5] A. Aboelhassan, A. M. Diab, M. Galea, and S. Bozhko, “Investigating electrical drive performance employing model predictive control and active disturbance rejection control algorithms,” in *Proc. 23rd Int. Conf. Elect. Mach. Syst.*, 2020, pp. 1379–1384, doi: [10.23919/ICEMS50442.2020.9291218](https://doi.org/10.23919/ICEMS50442.2020.9291218).
- [6] J. Gao, C. Gong, W. Li, and J. Liu, “Novel compensation strategy for calculation delay of finite control set model predictive current control in PMSM,” *IEEE Trans. Ind. Electron.*, vol. 67, no. 7, pp. 5816–5819, Jul. 2020.
- [7] S. Dai, J. Wang, Z. Sun, and E. Chong, “Deadbeat predictive current control for high-speed permanent magnet synchronous machine drives with low switching-to-fundamental frequency ratios,” *IEEE Trans. Ind. Electron.*, vol. 69, no. 5, pp. 4510–4521, May 2022.
- [8] J.-W. Jung, V. Q. Leu, T. D. Do, E.-K. Kim, and H. H. Choi, “Adaptive PID speed control design for permanent magnet synchronous motor drives,” *IEEE Trans. Power Electron.*, vol. 30, no. 2, pp. 900–908, Feb. 2015.
- [9] J. Xia, Z. Li, D. Yu, Y. Guo, and X. Zhang, “Robust speed and current control with parametric adaptation for surface-mounted PMSM considering system perturbations,” *IEEE J. Emerg. Sel. Topics Power Electron.*, vol. 9, no. 3, pp. 2807–2817, Jun. 2021.
- [10] T.-I. Yeom and D.-C. Lee, “Design of sliding-mode speed controller with active damping control for single-inverter dual-PMSM drive systems,” *IEEE Trans. Power Electron.*, vol. 36, no. 5, pp. 5794–5801, May 2021.
- [11] P. Lin, Z. Wu, K.-Z. Liu, and X.-M. Sun, “A class of linear-Nonlinear switching active disturbance rejection speed and current controllers for PMSM,” *IEEE Trans. Power Electron.*, vol. 36, no. 12, pp. 14366–14382, Dec. 2021.
- [12] F. Bu et al., “Speed ripple reduction of direct-drive PMSM servo system at low-speed operation using virtual cogging torque control method,” *IEEE Trans. Ind. Electron.*, vol. 68, no. 1, pp. 160–174, Jan. 2021.
- [13] M. F. Elmorshedy, W. Xu, F. F. M. El-Sousy, M. R. Islam, and A. A. Ahmed, “Recent achievements in model predictive control techniques for industrial motor: A comprehensive state-of-the-art,” *IEEE Access*, vol. 9, pp. 58170–58191, 2021.
- [14] P. Kakosimos and H. Abu-Rub, “Predictive speed control with short prediction horizon for permanent magnet synchronous motor drives,” *IEEE Trans. Power Electron.*, vol. 33, no. 3, pp. 2740–2750, Mar. 2018.
- [15] M. Liu et al., “Dual cost function model predictive direct speed control with duty ratio optimization for PMSM drives,” *IEEE Access*, vol. 8, pp. 126637–126647, 2020.
- [16] M. Shao, Y. Deng, H. Li, J. Liu, and Q. Fei, “Robust speed control for permanent magnet synchronous motors using a generalized predictive controller with a high-order terminal sliding-mode observer,” *IEEE Access*, vol. 7, pp. 121540–121551, 2019.
- [17] K. Wróbel, P. Serkies, and K. Szabat, “Model predictive base direct speed control of induction motor drive—Continuous and finite set approaches,” *Energies*, vol. 13, no. 5, 2020, Art. no. 1193, doi: [10.3390/en13051193](https://doi.org/10.3390/en13051193).
- [18] F. Wang, X. Mei, J. Rodriguez, and R. Kennel, “Model predictive control for electrical drive systems: An overview,” *Counselor Educ. Supervision Trans. Elect. Mach. Syst.*, vol. 1, no. 3, pp. 219–230, 2017, doi: [10.23919/TEMS.2017.8086100](https://doi.org/10.23919/TEMS.2017.8086100).
- [19] A. A. Abdelrauf, M. Abdel-Geliel, and E. Zakzouk, “Adaptive PID controller based on model predictive control,” in *Proc. Eur. Control Conf.*, 2016, pp. 746–751, doi: [10.1109/ECC.2016.7810378](https://doi.org/10.1109/ECC.2016.7810378).
- [20] L. M. A. Caseiro, A. M. S. Mendes, and S. M. A. Cruz, “Dynamically weighted optimal switching vector model predictive control of power converters,” *IEEE Trans. Ind. Electron.*, vol. 66, no. 2, pp. 1235–1245, Feb. 2019.
- [21] S. Vazquez et al., “An Artificial Intelligence approach for real-time tuning of weighting factors in FCS-MPC for power converters,” *IEEE Trans. Ind. Electron.*, vol. 69, no. 12, pp. 11987–11998, Dec. 2022.

- [22] C. R. Baier, R. O. Ramirez, E. I. Marciel, J. C. Hernández, P. E. Melín, and E. E. Espinosa, "FCS-MPC without steady-state error applied to a grid-connected cascaded H-bridge multi-level inverter," *IEEE Trans. Power Electron.*, vol. 36, no. 10, pp. 11785–11799, Oct. 2021.
- [23] D. Ye, J. Li, J. Chen, R. Qu, and L. Xiao, "Study on steady-state errors for asymmetrical six-phase permanent magnet synchronous machine fault-tolerant predictive current control," *IEEE Trans. Power Electron.*, vol. 35, no. 1, pp. 640–651, Jan. 2020.
- [24] A. Aboelhassan, S. Wang, Y. Mikhaylov, G. Buticchi, M. Galea, and S. Bozhko, "Discontinuous modulated model predictive control for low inductance high-speed electric drive applications," *IEEE Trans. Ind. Electron.*, to be published, doi: [10.1109/TIE.2023.3301532](https://doi.org/10.1109/TIE.2023.3301532).
- [25] Q. Wang et al., "A low-complexity optimal switching time-modulated model-predictive control for PMSM with three-level NPC converter," *IEEE Trans. Transp. Electrific.*, vol. 6, no. 3, pp. 1188–1198, Sep. 2020.
- [26] S. S. Yeoh, T. Yang, L. Tarisciotti, C. I. Hill, S. Bozhko, and P. Zanchetta, "Permanent-magnet machine-based starter-generator system with modulated model predictive control," *IEEE Trans. Transp. Electrific.*, vol. 3, no. 4, pp. 878–890, Dec. 2017.
- [27] L. Tarisciotti, P. Zanchetta, A. Watson, J. C. Clare, M. Degano, and S. Bifaretti, "Modulated model predictive control for a three-phase active rectifier," *IEEE Trans. Ind. Appl.*, vol. 51, no. 2, pp. 1610–1620, Mar. 2015.
- [28] M. Vijayagopal, P. Zanchetta, L. Empringham, L. de Lillo, L. Tarisciotti, and P. Wheeler, "Control of a direct matrix converter with modulated model-predictive control," *IEEE Trans. Ind. Appl.*, vol. 53, no. 3, pp. 2342–2349, May/Jun. 2017.
- [29] M. Ayala, J. Doval-Gandoy, J. Rodas, O. Gonzalez, R. Gregor, and M. Rivera, "A novel modulated model predictive control applied to six-phase induction motor drives," *IEEE Trans. Ind. Electron.*, vol. 68, no. 5, pp. 3672–3682, May 2021.
- [30] A. Aboelhassan, W. El Sayed, A. Hebala, M. Galea, and S. Bozhko, "Fault tolerant control strategy based on model predictive control and unscented kalman filter for permanent magnet synchronous motor," in *Proc. IEEE 16th Conf. Ind. Electron. Appl.*, 2021, pp. 153–159, doi: [10.1109/ICIEA51954.2021.9516257](https://doi.org/10.1109/ICIEA51954.2021.9516257).
- [31] A. Aboelhassan, M. Abdelgeliel, E. E. Zakzouk, and M. Galea, "Design and implementation of model predictive control based PID controller for industrial applications," *Energies*, vol. 13, no. 24, Dec. 2020, Art. no. 6594, doi: [10.3390/en13246594](https://doi.org/10.3390/en13246594).
- [32] Z. Kuang, B. Du, S. Cui, and C. C. Chan, "Speed control of load torque feedforward compensation based on linear active disturbance rejection for five-phase PMSM," *IEEE Access*, vol. 7, pp. 159787–159796, 2019.
- [33] C. Garcia, J. Rodriguez, S. Odhano, P. Zanchetta, and S. A. Davari, "Modulated model predictive speed control for PMSM drives," in *Proc. IEEE Int. Conf. Elect. Syst. Aircr., Railway, Ship Propulsion Road Veh. Int. Transp. Electrific. Conf.*, 2018, pp. 1–6, doi: [10.1109/ESARS-ITEC.2018.8607701](https://doi.org/10.1109/ESARS-ITEC.2018.8607701).
- [34] A. M. Diab et al., "Fast and simple tuning rules of synchronous reference frame proportional-integral current controller," *IEEE Access*, vol. 9, pp. 22156–22170, 2021.



**AHMED ABOELHASSAN** (Member, IEEE) received the M.Sc. degree in electrical and control engineering from the Arab Academy for Science, Technology, and Maritime Transport (AASTMT), Alexandria, Egypt, in 2016, and the Ph.D. degree in electrical and electronics engineering from the University of Nottingham, Ningbo, China, in 2023. He joined AASTMT in 2014 as an Assistant Lecturer. His research interests include model-based control algorithms, electrical drive applications, renewable energy systems, and industrial control.



**SHUO WANG** (Member, IEEE) received the Ph.D. degree in control science and engineering from Tongji University, Shanghai, China, in 2019.

From 2017 to 2018, he became a Visiting Researcher with Power Electronics, Machines and Control Group, University of Nottingham, Nottingham, U.K. He is currently working as a Senior Research Fellow with the University of Nottingham, Ningbo, China. His research interests include high-performance torque control, sensorless control, and flux-weakening control used for permanent magnet synchronous machines, synchronous reluctance machines, and permanent magnet-assisted synchronous reluctance machines.



**GIAMPAOLO BUTICCHI** (Senior Member, IEEE) received the M.Sc. degree in electronic engineering and the Ph.D. degree in information technologies from the University of Parma, Parma, Italy, in 2009 and 2013, respectively.

In 2012, he was a Visiting Researcher with the University of Nottingham, Nottingham, U.K. Between 2014 and 2017, he was a Postdoctoral Researcher with the University of Kiel, Kiel, Germany. He is currently a Professor of Electrical Engineering with the University of Nottingham, Ningbo, China.



**VASYL VARVOLIK** (Member, IEEE) received the B.Sc. and M.Sc. degrees in electrical engineering from the National Technical University of Ukraine "Igor Sikorsky Kyiv Polytechnic Institute," Kyiv, Ukraine, in 2016 and 2018, respectively. He is currently working toward the Ph.D. degree in electrical and electronics engineering with the University of Nottingham, Ningbo, China.

His research interests include high-fidelity simulation, parameter identification, torque ripple reduction, high-performance control of synchronous reluctance, and permanent magnet synchronous motor drives.



**MICHAEL GALEA** (Senior Member, IEEE) received the Ph.D. degree in electrical machine design from the University of Nottingham, Nottingham, U.K., in 2013.

He was a Full Professor of Electrical Machines and Drives with the University of Nottingham, in 2019. He is currently a Professor with the Department of Electrical Engineering, University of Malta, Msida, Malta.



**SERHIY BOZHKO** (Senior Member, IEEE) received the M.Sc. and Ph.D. degrees in electromechanical systems from the National Technical University of Ukraine, Kyiv, Ukraine, in 1987 and 1994, respectively.

Since 2000, he has been with the Power Electronics, Machines and Controls Research Group, University of Nottingham, Nottingham, U.K., where he is currently a Professor of Aircraft Electric Power Systems.